JMEPEG (2019) 28:4751–4761
https://doi.org/10.1007/s11665-019-04245-2

1059-9495/$19.00

Structural, Adhesion and Electrochemical Characterization of Electroless Plated Ni-P-Carbon Black Composite Films on API 5L X80 Steel

Mara Cristina Lopes de Oliveira, Olandir Vercino Correa, Rejane Maria Pereira da Silva, Nelson Batista de Lima, Jefferson Thadeu Dias de Oliveira, Leandro Antônio de Oliveira, and Renato Altobelli Antunes

(Submitted January 20, 2019; in revised form July 15, 2019; published online August 2, 2019)

In this work, composite Ni-P-carbon black coatings were obtained by electroless deposition on API 5L X80 substrates. The effect of carbon black on structural, adhesion and electrochemical properties of the plated samples was evaluated. Scanning electron microscopy analyses were carried out to examine the top surface and cross section of the films. Scratch tests were employed to evaluate coating adhesion properties. Potentiodynamic polarization tests were carried out to investigate the global electrochemical behavior of the deposited layers. Scanning electrochemical microscopy (SECM) was employed to measure local electrochemical activity over the coated surfaces. The carbon black concentration markedly affects the morphology, adhesion and electrochemical properties of the Ni-P-carbon black layers. The results point to an optimum carbon black content to achieve the best performance against corrosion. The coatings obtained at a carbon black concentration of 0.25 g L^{-1} provided the best protection ability. The results are discussed with respect to coating morphology, adhesion and electrochemical activity.

Keywords corrosion, Ni-P-carbon black composite films, scanning electrochemical microscopy

1. Introduction

Electroless Ni-P coatings are traditionally employed to improve the surface properties of metallic materials in several engineering applications such as for equipment for electronic, aerospace and chemical industries (Ref 1, 2). The pivotal role played by Ni-P layers as protecting agents for metallic substrates relies on their outstanding wear and corrosion resistances (Ref 3-5). Carbon steels, aluminum and magnesium alloys have been successfully employed as substrates for electroless deposition of Ni-P alloys (Ref 6-9).

In spite of its widespread usage, increasingly harsh environments trigger the need for electroless Ni-P films with even higher performance. In this respect, composite Ni-P coatings have been developed by incorporating a variety of particles with the aim of improving the surface hardness. Second-phase particles such as SiC, Al_2O_3, TiO_2, carbon nitride, ZrO_2 and SiO_2 have been incorporated into the Ni-P matrix promoting reinforcement and improving the wear behavior with respect to the conventional unfilled alloy (Ref 10-15).

Tailoring the surface properties of electroless nickel-based films is particularly important for applications in the oil and gas industries. Pipeline steels suffer from erosion-enhanced corrosion problems that reduce their lifetime (Ref 16). High-strength low-alloy (HSLA) steels are the primary material choice for pipeline manufacturing. These materials may greatly benefit from being internally coated with high-hardness coatings (Ref 17). Electroless Ni-P layers play a central role in this scenario (Ref 18).

Carbon-based fillers have gained interest as potential fillers for Ni-P composite coatings. Attractive frictional properties are the most important feature of such new nickel-based films, taking advantage of the intrinsic low friction coefficient of the carbon fillers (Ref 19, 20). Carbon black, in particular, can be exploited as a wear-reducing agent for composite materials. Although this capability has been traditionally explored for developing bulk polymer-carbon black composites (Ref 21-23), some instances of metallic-carbon black composite films can be found in the literature (Ref 20, 24). In these reports, though, the main focus is on the low electrical resistance of the carbon black-filled metallic coating. Its applicability as a protective layer against wear and corrosion of the metallic substrate is not reported. If one thinks of electroless Ni-P-carbon black composite films on HSLA pipeline steels, the literature is even scarcer. Although several reports on the preparation of Ni-P-carbon nanotubes coatings have been published (Ref 25-27), Ni-P-carbon black composite coatings have not been explored as a protective layer to increase both the corrosion and wear resistance of pipeline steels.

Scanning electrochemical microscopy (SECM) is a localized electrochemical technique in which a microelectrode tip is

Electronic supplementary material The online version of this article (https://doi.org/10.1007/s11665-019-04245-2) contains supplementary material, which is available to authorized users.

Mara Cristina Lopes de Oliveira, Jefferson Thadeu Dias de Oliveira, Leandro Antônio de Oliveira, and **Renato Altobelli Antunes**, Centro de Engenharia, Modelagem e Ciências Sociais Aplicadas (CECS), Universidade Federal do ABC (UFABC), Santo André, SP 09210-580, Brazil; and **Olandir Vercino Correa, Rejane Maria Pereira da Silva,** and **Nelson Batista de Lima**, Centro de Ciência e Tecnologia de Materiais (CCTM), Instituto de Pesquisas Energéticas e Nucleares (IPEN/CNEN-SP), São Paulo, SP 05508-000, Brazil. Contact e-mail: renato.antunes@ufabc.edu.br.

scanned over the metallic surface to probe specific electrochemical reactions. It has been employed to study localized corrosion processes in a variety of metals such as carbon steels, stainless steels, aluminum alloys and magnesium alloys (Ref 28-31). Passivation, pitting corrosion, underfilm corrosion, local corrosion spots at defective sites in coated metals and galvanic corrosion are some of the examples of possible SECM investigations (Ref 32). Notwithstanding, there are few studies on SECM analysis of pipeline steels (Ref 33). Up to the authors' knowledge, the use of SECM for electroless Ni-P-carbon black coatings has not been reported before.

The aim of the present work was to develop electroless Ni-P-carbon black composite coatings on API 5L X80 pipeline steel substrates and to assess the local electrochemical activity of the deposited films by SECM. Additionally, structural, morphological, adhesion and friction characteristics were examined by characterized by X-ray diffraction (XRD), scanning electron microscopy (SEM), confocal laser scanning microscopy (CLSM), scratch tests and dry sliding wear tests.

2. Experimental Details

2.1 Materials and Sample Preparation

The API 5L X80 pipeline steel plate (in wt.%: 0.04% C, 1.75% Mn, 0.20% Si, 0.02% P, 0.002% S, 0.065% Nb, 0.025% Al, 0.11% Cr, 0.025% V and balance Fe) used as the substrate for electroless deposition was kindly provided by Usiminas (Brazil). The as-received material was cut into small rectangular pieces (30 mm × 20 mm × 5 mm). These parts were used as substrates for deposition. Surface preparation was comprised of grinding with SiC waterproof paper up to grit 1200, followed by cleaning with alcohol, rinsing with deionized water and drying in a warm air stream provided by a conventional heat gun.

The composition of the Ni-P plating bath is displayed in Table 1. All chemicals for electroless deposition were pure analytical grade reagents. Three concentrations of carbon black (CB) particles (Vulcan XC 72 Cabot Corporation) were added to the bath 0.25 g L^{-1}, 0.50 g L^{-1} and 1.0 g L^{-1}. These films will be further named as CB-0.25, CB-0.50 and CB-1.0 throughout the text. The bath was magnetically stirred during the whole deposition procedure which lasted for 2 h. Alkaline cleaning was carried out before deposition by immersing the API 5L X80 samples in 10 wt.% NaOH solution at 50 °C for 10 min. Next, the samples were washed with deionized water.

Table 1 Composition and operating conditions of the plating bath for obtained the Ni-P-CB composite coatings

Reagent	Concentration, g L^{-1}
Nickel sulfate ($NiSO_4 \cdot 6H_2O$)	20
Nickel hypophosphite ($Na_2H_2PO_2 \cdot H_2O$)	20
Citric acid ($Na_3C_6H_5O_7 \cdot 2H_2O$)	35
Ammonium sulfate ($(NH_4)_2SO_4$)	40
Operating conditions	
pH	9.0
Temperature	88 °C
Magnetic stirring	

Surface activation was accomplished in 50% vol. H_2SO_4 solution at room temperature for 30 s. The samples were, then, washed again with deionized water and finally immersed in the Ni-P-CB plating bath. At the end of the deposition time, the samples were thoroughly washed with deionized water and dried in a warm air stream using a heat gun.

The as-deposited samples were subject to annealing in a tubular furnace at 400 °C for 1 h under argon atmosphere. This heat treatment is frequently adopted to increase the hardness of electroless Ni-P layers by promoting the precipitation of nickel phosphides (Ref 34).

2.2 Coating Characterization

XRD patterns of the Ni-P and Ni-P-CB coatings were acquired using a Rigaku DMAX-2000 diffractometer, operating with Cu-kα radiation in the θ-2θ configuration in the 2θ range from 20° to 70°. SEM micrographs of the top surfaces and cross-sectional views were obtained using Hitachi TM3000 and Jeol JMS-6010LA microscopes, respectively. Energy-dispersive X-ray analysis (EDS) was carried out to detect the elemental composition at the coating/substrate interface. CLSM analysis (Olympus, LEXT OLS4100) was employed to examine the scratch region and measure specific topographic features after subjecting the samples to scratch tests.

The samples were also subject to scratch tests to evaluate the influence of carbon black concentration in the bath on the adhesion strength of the plated layers. The testing method was comprised of a continuous load increase step with a loading rate of 2 N min^{-1}. The total scratch length was 10 mm. The applied normal force was in the rage from 1 to 38 N. The scratch velocity was 0.5 mm s^{-1}. The tests were conducted using a Ducom Instruments T101 apparatus equipped with a Rockwell C-type diamond tip.

Dry sliding reciprocating wear tests of the conventional Ni-P and Ni-P-CB coatings were carried out using a nanotribometer (Anton Paar, NTR^2). The tests were conducted using a 2-mm-diameter chromium steel ball as the counter body. The maximum normal load was 20 mN which was selected in order to obtain the friction response of the deposited films. The number of cycles was 3600 with a frequency of 2 Hz and amplitude of 1.5 mm. These conditions were selected to allow clear distinguishing between the friction properties of the different nickel-based films.

2.3 Electrochemical Studies

2.3.1 Potentiodynamic Polarization. Potentiodynamic polarization tests were conducted in a Autolab M101 potentiostat/galvanostat. A conventional three-electrode cell configuration was employed with a platinum wire as the auxiliary electrode, Ag/AgCl as reference and the Ni-P-CB-coated samples as the working electrodes. The electrolyte was a 3.5 wt.% solution at room temperature Initially, the open-circuit potential was monitored for 1 h to ensure a steady-state condition. Next, the samples were subject to potentiodynamic polarization from − 0.3 V with respect to the open-circuit potential up to + 1.0 $V_{Ag/AgCl}$ at a scan rate of 1 mV s^{-1}.

2.3.2 SECM. The SECM scan was performed using a commercial apparatus by Sensolytics. The tip was a glass-insulated Pt microelectrode with 10 µm diameter. A saturated calomel electrode (SCE) was the reference electrode, and a Pt wire was the auxiliary electrode. The specimens were mounted

horizontally facing upwards. The tip was positioned at a height of 30 μm above the substrate. The potentials of tip and specimen were controlled with a bipotentiostat coupled to the SECM system. The measurements were taken with the specimen at the open-circuit potential using a 0.1 M NaCl solution at room temperature as the electrolyte. The instrument was operated in the generation-collection mode (G-C). The tip was biased at + 600 $mV_{Ag/AgCl}$ to detect the oxidation reaction of Fe^{2+} to Fe^{3+} which is typical of the corrosion process of ferrous alloys (Ref 35). Tip velocity was 10 $\mu m.s^{-1}$. The scanned area was 500 μm × 500 μm.

3. Results and Discussion

3.1 Structural and Morphological Characterization

XRD patterns of the as-plated and annealed Ni-P and Ni-P-CB coatings are shown in Fig. 1. In the as-plated condition, there is an intense Ni (111) reflection at approximately 44.5° (JCPDS 00-004-0850) whose intensity is gradually reduced as the CB content increases (Fig. 1a). Furthermore, the crystalline peak becomes broader with CB addition, indicating the amorphous character of the as-plated composite coatings. The crystalline peak is completely absent for the CB-1.0 film. Similar results have been reported for electroless Ni-P-carbon nanotube coatings, implying that by adding the carbon-based filler, amorphization is enhanced (Ref 36, 37).

The crystalline character of the electroless deposited films was enhanced after annealing at 400 °C for 1 h, as shown in Fig. 1(b). Several crystalline peaks are observed after the heat treatment due to precipitation of Ni_3P crystallites ((JCPDS 01-089-2743) in the nickel matrix, as reported by several authors (Ref 38-40). It is evident, though, that the crystalline character is markedly reduced with CB addition as denoted by the strong reduction of the intensity of the Ni (200) reflection at 51.84°.

Surface morphology of the Ni-P-CB composite coatings was examined by SEM analyses. Figure 2 displays SEM micrographs of the top surfaces for the Ni-P and Ni-P-CB coatings in the annealed condition.

A typical nodular morphology is observed for the Ni-P coating (Fig. 2a). It is sustained for the CB-containing films. The nodular growth has been reported for electroless nickel deposits, being related to a nucleation and growth process during film formation (Ref 41, 42). The spherical shape of the nodules is due to the autocatalytic reaction during electroless deposition with the participation of sodium hypophosphite (Ref 43). Small nodules are favored for high nucleation rates, whereas the nodules size tends to increase for lower nucleation rates (Ref 44). Fayyad et al. (Ref 13) have found that addition of small carbon nitride particles decreases the nodules size of electroless Ni-P coatings. Xu et al. (Ref 45) observed that Ni-P-carbon nanotube composite coatings exhibited smaller nodule size when compared to binary Ni-P films, thereby revealing a higher nucleation rate associated with the high surface energy of the carbon nanotubes. Lee (Ref 46) has reported that TiO_2 and carbon nanotubes increased the fineness of the typical nodular grains of electroless Ni-P coatings. Sadeghzadeh-Attar et al. (Ref 47) identified a reduction in the nodule size of Ni-P composite coating by adding small SiO_2 particles.

The nodule size was reduced for the Ni-P-CB composite coatings with respect to the conventional binary Ni-P layer. A similar effect was reported for composite electroless Ni-P-Al_2O_3 and Ni-B-SiO_2 films (Ref 48, 49). The small filler particles tend to restrict the nodular growth by agglomerating at nodule boundaries, thus restricting the growth rate. Some defective areas (pointed by arrows) are observed in the SEM micrographs of the CB-containing films (Fig. 2b, c and d) which are likely to be due to such agglomerating effect. Moreover, surface compactness can be perceived for the CB-0.25 sample (Fig. 2a) which is less defective than the CB-0.50 (Fig. 2c) and CB-1.0 (Fig. 2d) deposits.

The thickness of the deposited layers was assessed by examining cross-sectional SEM micrographs and their corresponding EDS mapping. A representative result is displayed in Fig. 3 for the Ni-P film. The results obtained for the Ni-P-B films are very similar and are provided as supplementary file. The coating layer is indicated by the regions enriched in Ni (Fig. 3b) and P (Fig. 3c) whose thickness is approximately 5 μm. The thicknesses of the composite films were very close to that, varying between 4 and 5 μm. In this respect, the deposition rate was not affected by the carbon black particles added to the plating solution. The interface between film and the steel substrate was relatively smooth for all conditions, as exemplified for the Ni-P in Fig. 3. The substrate region is indicated by the Fe-rich part of the image shown in Fig. 3(d). It is not possible to identify an interdiffusion layer between the film and the substrate. This aspect is frequently reported for

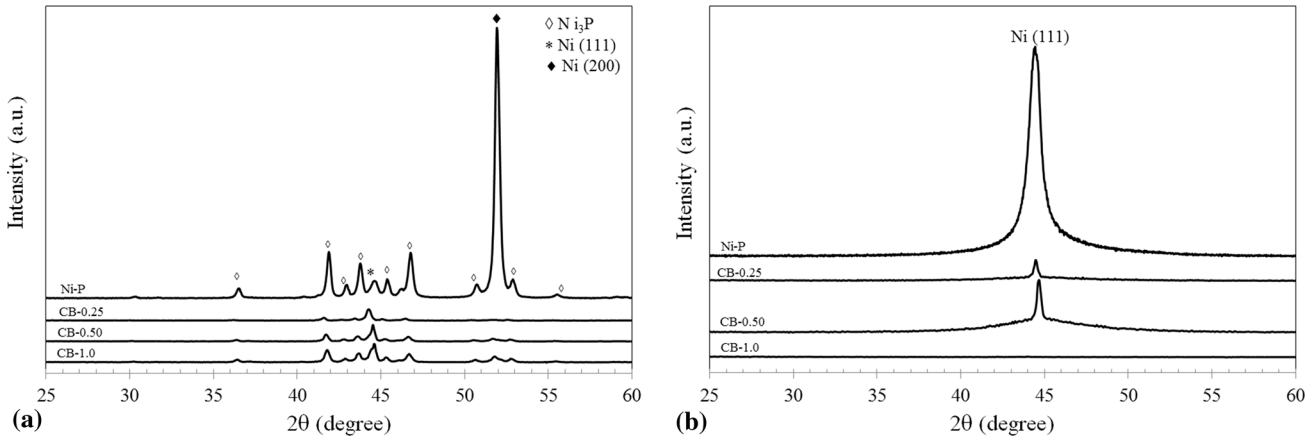

Fig. 1 XRD patterns of the Ni-P and Ni-P-CB coatings: (a) as-plated; (b) annealed at 400 °C for 1 h

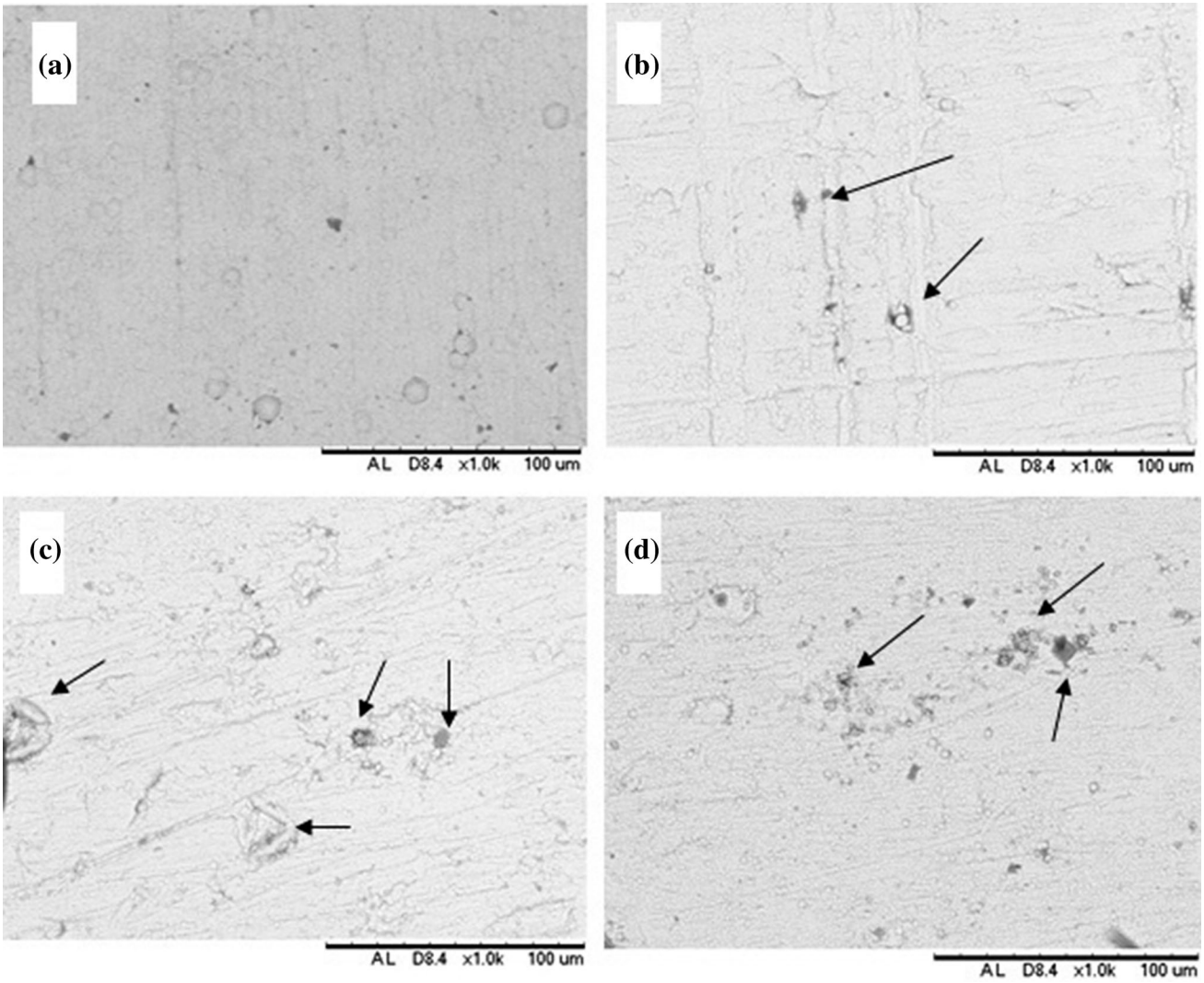

Fig. 2 SEM micrographs of the top surfaces of the annealed coatings: (a) Ni-P; (b) CB-0.25; (c) CB-0.50; (d) CB-1.0. Defective sites are indicated by arrows

electroless Ni-P films (Ref 40), but the diffusion of elements from the substrate to the coating layer depends on the temperature employed for the annealing treatment of the coated samples. Temperatures around 600 °C favor the formation of the interdiffusion layer (Ref 50). As the annealing temperature was 400 °C for the coatings developed in the present work, interdiffusion would not be favored.

3.2 Scratch Test

In order to evaluate the effect of the carbon black particles incorporated into the Ni-P layer on its adhesion properties, the samples were subject to scratch tests. CLSM micrographs of the scratched region and the corresponding transverse profiles are shown in Fig. 4. The markings over the CLSM micrographs indicate where the transverse profiles were measured for each sample. The lines were placed over the same region of the scratch in order to measure the scratch dimensions upon the same load level. This is an important procedure, since the scratch tests were not carried out at constant loads but rather using a continuous load increase method, as described in Sect. 2.2. As such, by taking the scratch dimensions at the same region over the scratch, we guarantee that they were measured at the same load level. In this respect, any difference would arise from the surface properties of the deposited layers, especially their adherence to the steel substrate. The scratch dimensions are displayed in Table 2. The data reveal that both the width and depth of the scratch were reduced by adding the carbon black particles to the Ni-P matrix. In fact, the penetration depth was significantly lower for the composite coatings compared to the conventional Ni-P film. In this respect, the binary Ni-P layer is less resistant to the penetration of the indenter during the scratch test, presenting a higher damage area which, in turn, is an indicative of poor adhesion properties in the scratch test (Ref 51). Electroless nickel coatings are annealed at temperatures close to 400 °C such as those evaluated in the present work as reported to be brittle (Ref 52, 53). In this case, the plastic deformation during the scratch test is mainly absorbed by the metallic substrate rather than by the brittle coating (Ref 54). By increasing the CB particles loading, the penetration depth gradually decreases.

Adhesion properties could be qualitatively assessed from the micrographs shown in Fig. 4. Adhesion failure can be perceived by the presence of the black region between the scratch

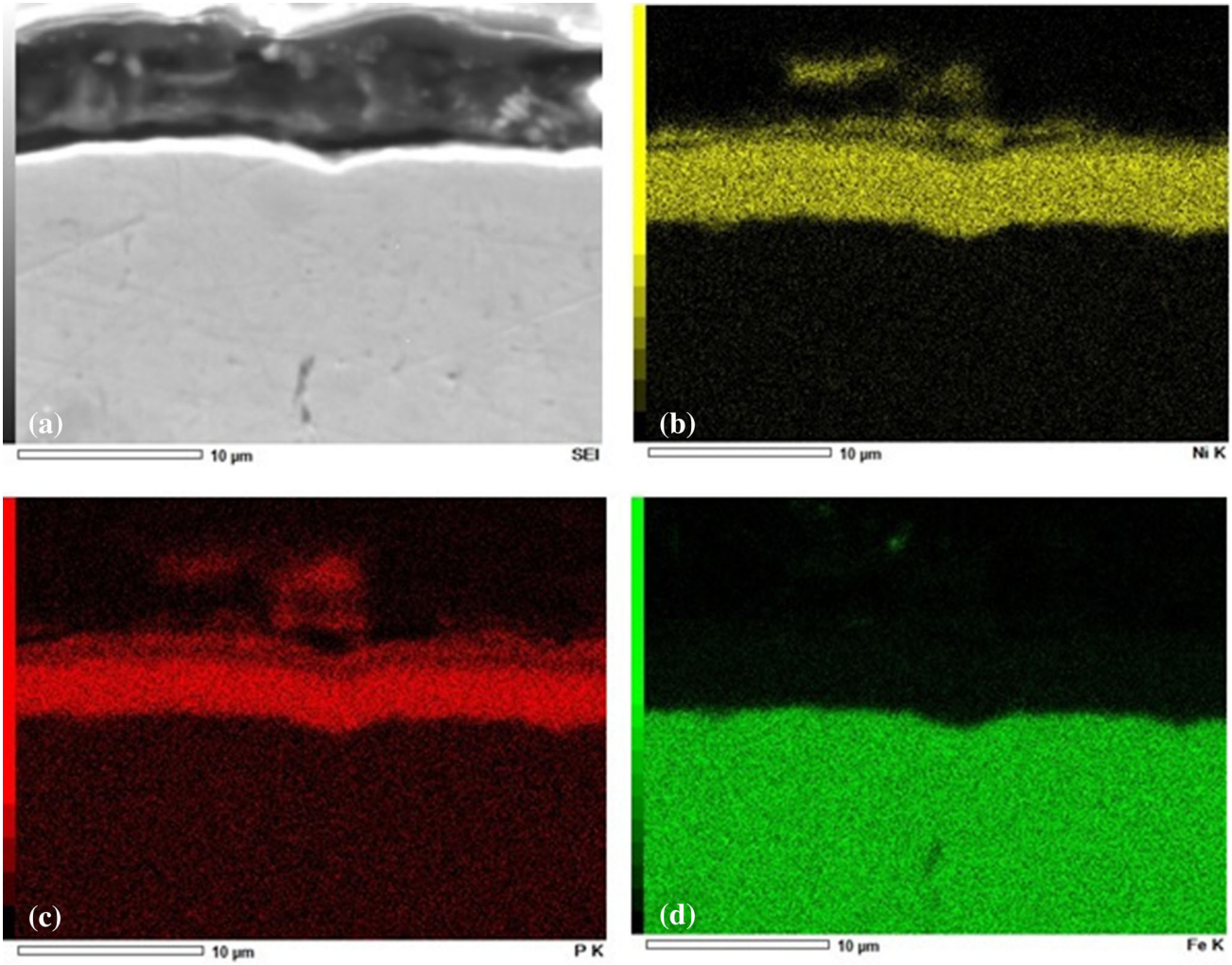

Fig. 3 EDS mapping of the cross sections for the annealed Ni-P film: (a) SEM micrograph; (b) Ni; (c) P; (d) Fe

and the coating layer. The scratch is located at middle of the 3D view (brighter region). Its interface with the unscratched surface is smooth for the CB-0.25 samples as indicated in Fig. 4(b). The coating is not delaminated over the scratch. For the Ni-P film, in turn, the interface with the unscratched surface is not as smooth as that of the CB-0.25 sample and the coating delaminated over the scratch length, as it can be perceived by the dark regions following the scratch line at the vicinity of the undamaged part of the film.

As mentioned above, the ductile character of the coatings was decreased for the higher-loading samples (CB-0.50 and CB-1.0), as indicated by the reduction in penetration depth. The morphological aspects of the scratched region were affected as well. As shown in Fig. 4(c), the scratch itself is shallower for the CB-0.50 when compared to C-0.25 (see the width dimensions in Table 2). Notwithstanding, the interface between the scratch and the unscratched surface is characterized by a wide delaminated region (dark region between bright scratch at the middle of the micrograph and the undamaged coating) for the CB-0.50 film. The same finding can be perceived for the CB-1.0 sample (Fig. 4d). These results suggest that adhesion is sacrificed as the carbon black content in the film increases. This effect has been reported for epoxy-carbon black composite coatings. Both the hydrophobic nature of the carbon black particles and its agglomeration at higher loading are responsible for decrease of adhesion between the coating and substrate (Ref 55). Well-dispersed particles are related to good adhesion properties which can be more easily attained at low filler loadings. The results obtained from the scratch tests point that the best adhesion properties were obtained for the CB-0.25. There is, therefore, an optimum content of the carbon black particles to enhance both the mechanical and adhesion properties of the Ni-P coatings.

3.3 Dry Sliding Wear Tests

The variation of the coefficient of friction (COF) with the sliding distance during dry sliding wear tests of the Ni-P and Ni-P-CB coatings is shown in Fig. 5. The COF of the conventional Ni-P film was higher than for the composite Ni-P-CB coatings throughout the whole test. Moreover, it increased at a faster rate at the beginning of the test and did not reach a steady state up to the end of the monitoring period. The COF was gradually decreased by incorporating the carbon black nanoparticles into the Ni-P matrix during electroless deposition. The variation of the COF with the sliding distance for Ni-P-CB composite coatings reached a steady-state condition. Similar results have been reported by Suzuki et al. (Ref

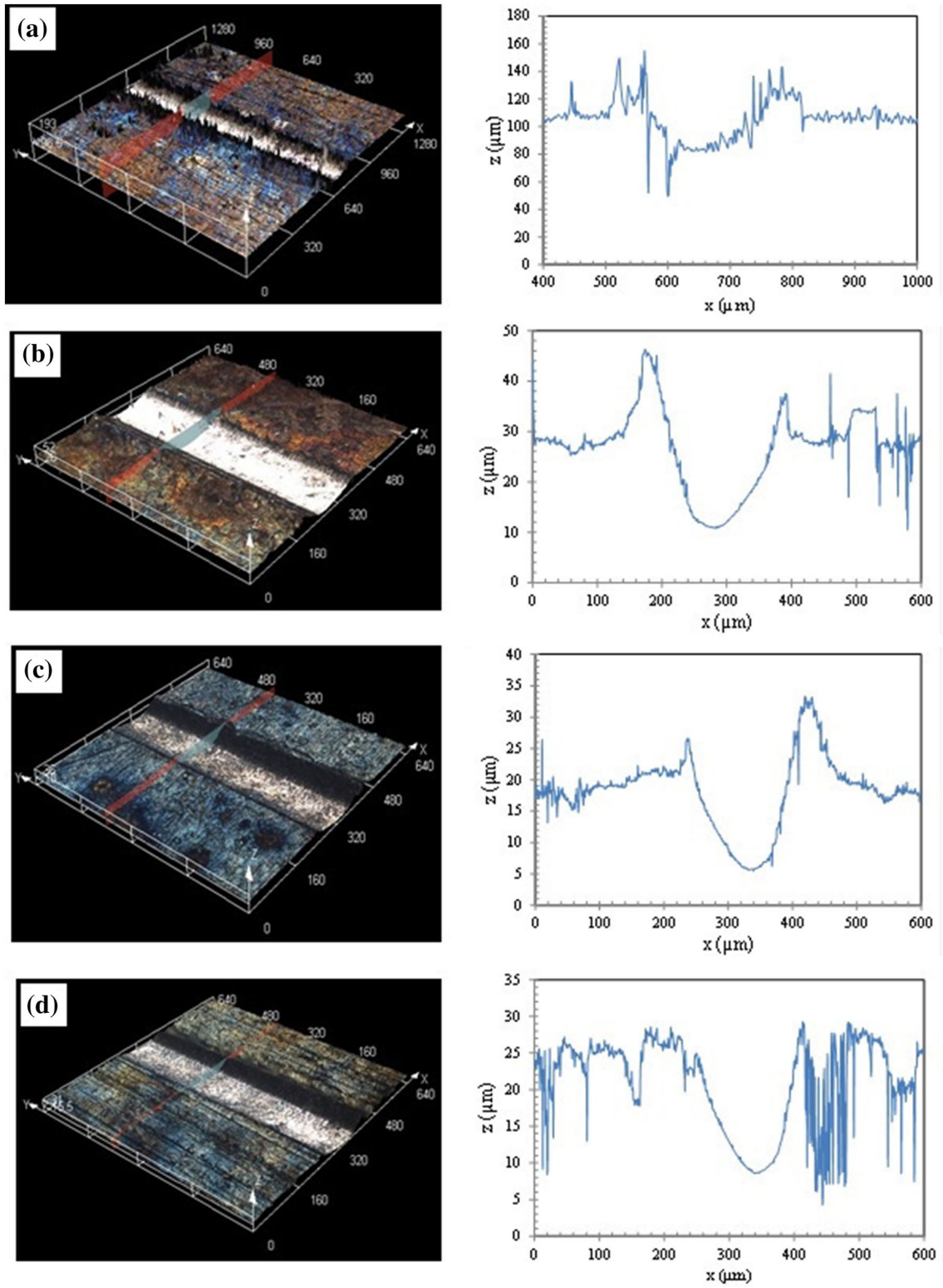

Fig. 4 CLSM micrographs of the scratched region and the corresponding transverse profile at the line marked over the scratch: (a) Ni-P; (b) CB-0.25; (c) CB-050 and (d) CB-1.0

56) for Ni-P-carbon black coatings obtained by electrodeposition. The COF decrease was proportional do the carbon black content in the film. The results shown in Fig. 5 follow the same trend. The COF of the CB-0.25 sample increased up to 6 m and then reached a steady-state condition. The increase was slower than for the binary Ni-P film and the COF values were lower during the whole test. The COF values were even lower for the CB-0.50 sample, and the steady-state condition was reached at a shorter sliding distance. The COF variation was very smooth during the whole monitoring period for the CB-1.0 and the values were the lowest ones among all samples. These results point a lubricating action of the carbon black nanoparticles

which was also reported in the work by Suzuki et al. (Ref 56) and for other Ni-P coating reinforced with carbon-based fillers (Ref 57). The friction properties of the Ni-P film can be optimized by the CB particles.

3.4 Electrochemical Behavior

3.4.1 Potentiodynamic Polarization. The corrosion properties of the annealed Ni-P-CB coatings were assessed by potentiodynamic polarization tests. The results are shown in Fig. 6. The tests were conducted in 3.5 wt.% NaCl solution at room temperature. The values of corrosion potential (E_{corr}) and corrosion current density (i_{corr}) were determined from these curves using the Tafel extrapolation method, considering only the cathodic branches. The data are displayed in Table 3.

Table 2 Scratch dimensions of the Ni-P and Ni-P-CB coatings

Sample	Width, µm	Maximum depth, µm
Ni-P	253	102
CB-0.25	211	36
CB-0.50	185	28
CB-1.0	179	20

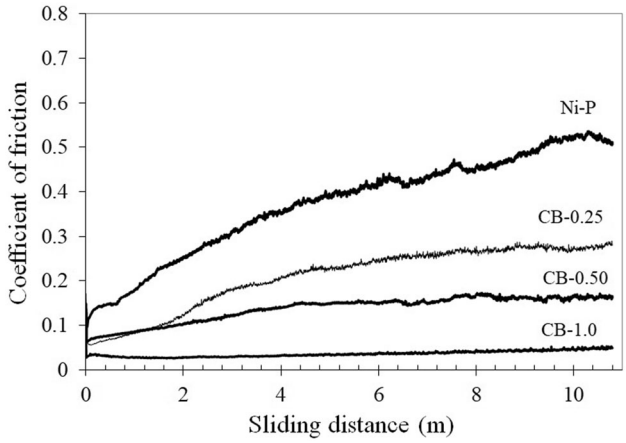

Fig. 5 Variation of the coefficient of friction with the sliding distance during dry sliding wear tests of the Ni-P and Ni-P-CB coatings

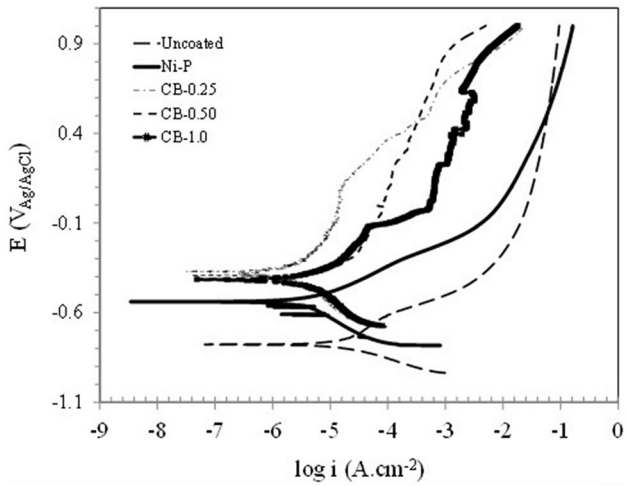

Fig. 6 Potentiodynamic polarization curves of the Ni-P and Ni-P-CB coatings

The uncoated substrate presents the highest corrosion susceptibility as denoted by its low corrosion potential with respect to all coated samples. In addition, its high i_{corr} indicates that corrosion evolves quickly. The polarization curve did not present signs of passivity, revealing the non-protective character of the corrosion products formed during anodic dissolution. The conventional Ni-P, in turn, presented a significant decrease of i_{corr}, although it does not passivate as well as the uncoated steel. The corrosion potential is shifted to more anodic values, indicating its lower corrosion susceptibility. This result is in agreement with the literature. Sharma and Singh (Ref 11) have also found that electroless Ni-P films increased the corrosion potential of a mild steel substrate and reduced its corrosion current density, showing a typically active polarization behavior.

The electrochemical response of the coated substrate was modified by incorporating the carbon black particles into the Ni-P matrix. The corrosion potentials of all Ni-P-carbon black-coated samples were shifted to more anodic values, indicating the noble character of the composite coatings and its lower corrosion susceptibility when compared to the conventional Ni-P film and the uncoated substrate. The polarization curves presented a passive region, independently of the carbon black loading. The CB-0.25 sample presented the lowest value of i_{corr} and the highest E_{corr}, indicating it is the most corrosion resistant condition. By increasing the carbon black concentration, the values of i_{corr} increased and E_{corr} decreased, suggesting that the corrosion protection ability of the composite coatings is hampered as the filler concentration surpasses 0.25 g L^{-1}. This can be promptly perceived by the higher anodic current in the passive region for the CB-0.50 and CB-1.0 samples, as well as by their higher values of i_{corr}. The higher electrochemical activity of the CB-050 and CB-1.0 samples can be related to coating morphology and adhesion. As shown in Fig. 2, the surface of these samples is more defective than that of CB-0.25. The defective sites can act as preferential paths for electrolyte penetration. The anodic currents would, therefore, increase due to faster substrate dissolution through the coatings defects. As shown in Sect. 3.2, adhesion of the composite coatings was also decreased for higher filler contents. Thus, it can be inferred that there is an optimum carbon black content to provide good corrosion protection ability to the composite coating. Similar findings have been reported by Ghasemi-Kharizsangi et al. (Ref 55). They studied the effect of carbon black concentration on the corrosion resistance of epoxy-carbon black composite coatings applied on mild steel. The corrosion protective ability

Table 3 Electrochemical parameters determined from the potentiodynamic polarization curves

Sample	E_{corr}, $mV_{Ag/AgCl}$	i_{corr}, µa cm^{-2}
Uncoated	− 778	203
Ni-P	− 540	4.17
CB-0.25	− 392	2.66
CB-0.50	− 421	3.63
CB-1.0	− 415	4.15

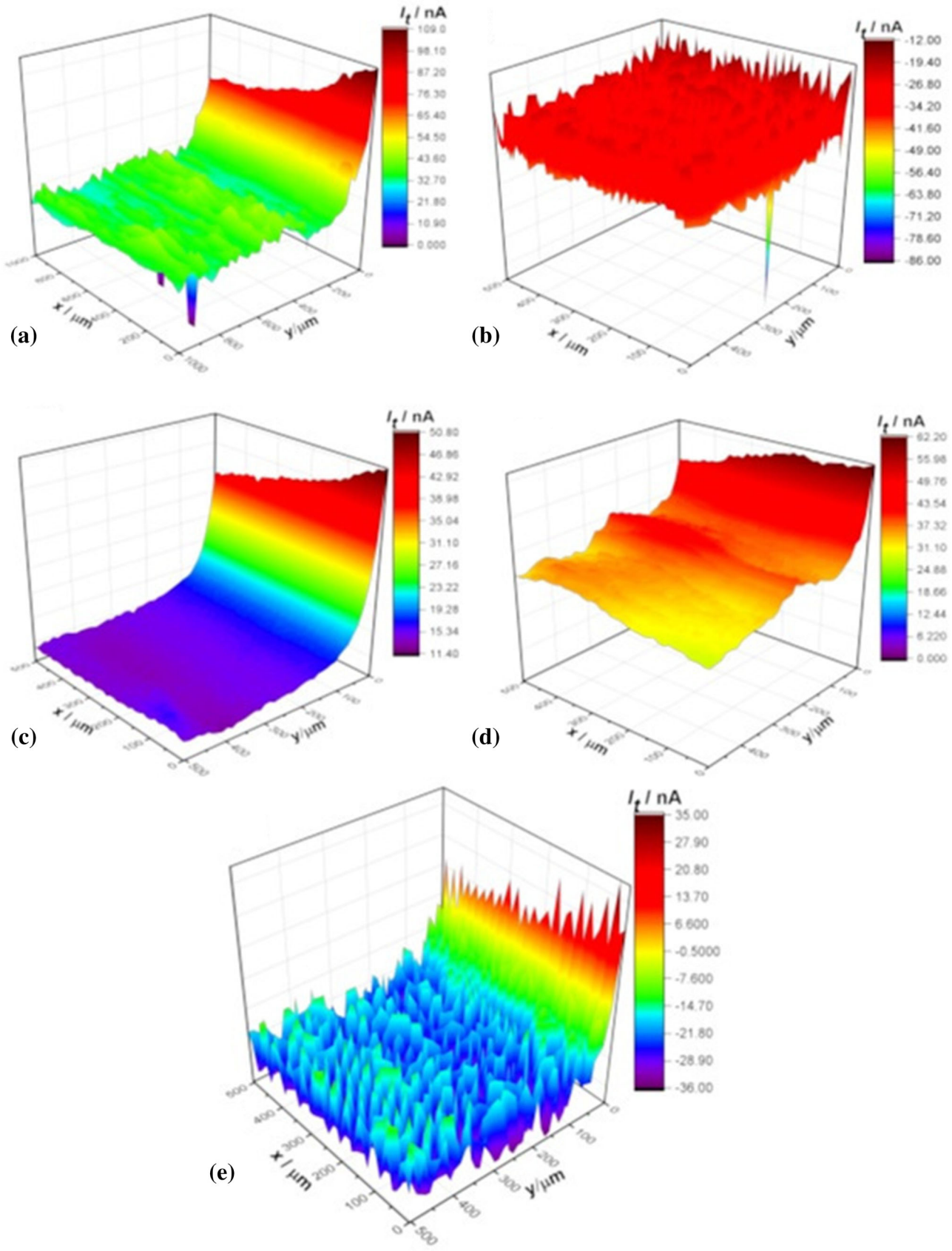

Fig. 7 SECM maps recorded over the substrate and coated samples: (a) Uncoated; (b) Ni-P; (c) CB-0.25; (d) CB-0.50; (e) CB-1.0. The substrate is at open circuit. The tip is biased at + 600 $mV_{Ag/AgCl}$

was dependent on the carbon black content added to the epoxy resin. At the optimum concentration, the carbon black particles present a barrier effect, increasing its corrosion resistance. Similar effects have been reported for Ni-P-Al_2O_3 (Ref 11), Ni-P-SiO_2 (Ref 58), Ni-P-carbon nanotubes (Ref 37) and Ni-P-diamond nanoparticles (Ref 59) composite coatings. The small filler particles fill surface defects such as cracks and pores, thereby increasing the corrosion resistance. However, as the filler concentration increases, the small carbon black particles tend to agglomerate. As a result, the barrier effect of these particles is less pronounced, since they are not evenly distributed over the matrix, decreasing its adhesion to the substrate. Consequently, corrosion susceptibility increases. The electrochemical activity of the coated samples was further evaluated by SECM, as shown in the next section.

3.4.2 SECM Maps. Figure 7 displays SECM 3D current maps of the annealed Ni-P and Ni-P-CB samples at open-circuit potential immersed in 0.1 M NaCl solution at room temperature. The tip is biased at + 600 mVAg/AgCl. The uncoated substrate was also tested for comparison.

Fe^{2+} species are expected to form at defective sites in the coating layer as a result of anodic dissolution of the ferrous substrate employed in the present work under the near neutral conditions of the 0.1 M NaCl solution (Ref 60, 61). The current values are, thus, expected to rise at the sites of Fe^{2+} formation. The highest current values were recorded for the uncoated substrate, as displayed in Fig. 7(a). This indicates that there are more Fe^{2+} ions available for oxidation into Fe^{3+} at the tip. When the substrate is covered by the conventional Ni-P film (Fig. 7b), the current values are cathodic over the whole scanned area. The surface of the coated substrate has, therefore, lower electrochemical activity when compared to the bare substrate. Another interesting effect is that as the concentration of Fe^{2+} ions emanating from the Ni-P-coated substrate is low, they can be more easily oxidized into Fe^{3+} before diffusing into the bulk electrolyte. Hence, cathodic currents would arise from regions in the probed surface where the Fe^{3+} ions are being produced. A similar effect was reported by Izquierdo et al. (Ref 62). Although the cathodic currents have small magnitudes over the surface of the Ni-P-coated sample, the presence of such regions would indicate the propensity of the Ni-P layer to undergo Fe^{2+} oxidation reaction at its defective sites.

The CB-0.25 map (Fig. 7c) is characterized by anodic currents with very small magnitude over the probed area. The maximum activity, corresponding to the regions where the Fe^{2+} electroactive species present higher concentration, is at the right part of the image, suggesting it is not homogeneously distributed over the area. As described by Zhao et al. (Ref 61), this effect could be due to movement of the tip during the linescans performed to acquire the current map over the sample surface. As a result, the tip can agitate the solution, shifting the profiles of maximum concentration for the electroactive species. Notwithstanding, the anodic currents are lower than that of the substrate. A similar behavior was observed for the CB-0.50 map (Fig. 7d) but the anodic currents are higher than those of the CB-0.25 sample, revealing its higher activity. This behavior is in agreement with the potentiodynamic polarization tests and can be related to the more defective surface state of the CB-0.50 sample, as shown in Fig. 2.

Intense current fluctuations were detected for the CB-1.0 sample (Fig. 7e) which can be associated with localized anodic dissolution of the probed surface, as suggested by Esmaeili et al. (Ref 35). In this respect, SECM reveals that the increase in carbon black loading in the deposition bath led to an increment of the electrochemical activity of the Ni-P-CB coatings. This behavior can be associated with the more difficult dispersion of the carbon black particles during electroless deposition, giving rise to more defective sites in the coating layer, as confirmed by the SEM micrographs shown in Fig. 2. The electrochemical behavior of the composite Ni-P-CB is closely related to this morphological aspect which must be carefully controlled by adding proper amounts of the carbon filler into solution during the deposition process.

4. Conclusions

Composite Ni-P-carbon black coatings were successfully obtained by electroless deposition. The carbon black concentration in the bath played a central role in the coating morphology, adhesion and electrochemical behavior. Although the thickness of the deposited layer was not dependent on the CB loading, the presence of defects on the coating surface was related to the filler concentration. Surface defects were detected for CB loading above 0.25 g L^{-1}. Both the electrochemical activity and adhesion were decreased for the coatings produced in baths with higher CB concentrations. The best corrosion protection ability was obtained for the films obtained at a CB loading of 0.25 g L^{-1}, showing good adhesion and fewer surface defects. SECM proved to be a powerful tool to assess the electrochemical activity of the composite coatings.

Acknowledgments

Usiminas (Brazil) is acknowledged for providing the API 5L X80 plate used in the present work. This work was funded by CNPq (Process 470944/2013-7).

References

1. H. Liu, F. Viejo, R.X. Guo, S. Glenday, and Z. Liu, Microstructure and Corrosion Performance of Laser-Annealed Electroless Ni-W-P Coatings, *Surf. Coat. Technol.*, 2010, **204**, p 1549–1555
2. Q. Wang, M. Callisti, A. Miranda, B. McKay, I. Deligkiozi, T.K. Milickovic, A. Zoikis-Karathanasis, K. Hrissagis, L. Magagnin, and T. Polcar, Evolution of Structural, Mechanical and Tribological Properties of Ni-P/MWCNT Coatings as a Function of Annealing Temperature, *Surf. Coat. Technol.*, 2016, **302**, p 195–201
3. A.M. Pillai, A. Rajendra, and A.K. Sharma, Electrodeposited Nickel-Phosphorus (Ni-P) Alloy Coating: An In-Depth Study of Its Preparation, Properties, and Structural Transitions, *J. Coat. Technol. Res.*, 2012, **9**, p 785–797
4. F.S. Goettems and J.Z. Ferreira, Wear Behavior of Electroless Heat Treated Ni-P Coatings as Alternative to Electroplated Hard Chromium Deposits, *Mater. Res.*, 2017, **20**, p 1300–1308
5. K. HariKrishnan, S. John, K.N. Srinivasan, J. Praveen, M. Ganesan, and P.M. Kavimani, An Overall Aspect of Electroless Ni-P Depositions—A Review Article, *Metall. Mater. Trans. A*, 2006, **37**, p 1917–1926
6. B. Panja and P. Sahoo, Tribo-Corrosion Behavior of Electroless Ni-P Coatings in Alkaline Corrosive Environment, *Port. Electrochim. Acta*, 2014, **32**, p 303–313
7. M. Sahal, Characterization of Ni-P Coating on AZ91D Magnesium Alloy with Surfactants and Nano-additives, *J. Magnes. Alloys*, 2014, **2**, p 293–298

8. W. Qin, Microstructure and Corrosion Behavior of Electroless Ni-P Coatings on 6061 Aluminum Alloys, *J. Coat. Technol. Res.*, 2011, **8**, p 135–139
9. A.A. Ashtiani, S. Faraji, S.A. Iranagh, and A.H. Faraji, The Study of Electroless Ni-P Alloys with Different Complexing Agents on Ck45 Steel Substrate, *Arab. J. Chem.*, 2017, **10**, p S1541–S1545
10. M. Islam, M.R. Azhar, Y. Khalid, R. Khan, H.S. Abdo, M.A. Dar, O.R. Oloyede, and T.D. Burleigh, Electroless Ni-P/SiC Nanocomposite Coatings with Small Amounts of SiC Nanoparticles for Superior Corrosion Resistance and Hardness, *J. Mater. Eng. Perform.*, 2015, **25**, p 4835–4843
11. A. Sharma and A.K. Singh, Electroless Ni-P and Ni-P-Al_2O_3 Nanocomposite Coatings and Their Corrosion and Wear Resistance, *J. Mater. Eng. Perform.*, 2013, **22**, p 176–183
12. P. Gadhari and P. Sahoo, Effect of TiO_2 Particles on Micro-hardness, Corrosion, Wear and Friction of Ni-P-TiO_2 Composite Coatings at Different Annealing Temperatures, *Surf. Rev. Lett.*, 2015, **22**, p 1550082
13. E.M. Fayyad, A.M. Abdullah, M.K. Hassan, A.M. Mohamed, C. Wang, G. Jarjoura, and Z. Farhat, Synthesis, Characterization, and Application of Novel Ni-P-Carbon Nitride Nanocomposites, *Coatings*, 2018, **8**, p 8010037
14. Y. Yang, W. Chen, C. Zhou, H. Xu, and W. Gao, Fabrication and Characterization of Electroless Ni-P-ZrO_2 Nano-composite Coatings, *Appl. Nanosci.*, 2011, **1**, p 19–26
15. S. Sadreddini and A. Afshar, The Effect of Heat Treatment on Properties of Ni-P-SiO_2 Nano-composite Coating, *Prot. Met. Phys. Chem. Surf.*, 2016, **52**, p 492–499
16. C. Wang, Z. Farhat, G. Jarjoura, M. Hassan, and A.M. Abdullah, Indentation and Erosion Behavior of Electroless Ni-P Coating on Pipeline Steel, *Wear*, 2017, **376–377**, p 1630–1639
17. M.M. Mirza, E. Rasu, and A. Desilva, Surface Coatings on Steel Pipes Used in Oil and Gas Industries—A Review, *Am. Chem. Sci. J.*, 2016, **13**, p 1–23
18. C. Wang, Z. Farhat, G. Jarjoura, M.K. Hassan, A.M. Abdullah, and E.M. Fayyad, Investigation of Fracture Behavior of Annealed Electroless Ni-P Coating on Pipeline Steel Using Acoustic Emission Methodology, *Surf. Coat. Technol.*, 2017, **326A**, p 336–342
19. W. Brostow, M. Keselman, I. Mironi-Harpaz, M. Narkis, and R. Peirce, Effects of Carbon Black on Tribology of Blends of Poly(vinylidene fluoride) with Irradiated and Non-irradiated Ultrahigh Molecular Weight Polyethylene, *Polymer*, 2005, **46**, p 5058–5064
20. L. Stappers, C.N. Ngoy, W. Zhang, M. Toben, and J. Fransaer, Electrodeposition of Silver-Carbon Coatings with Low Contact Resistance and Wear Rate, *J. Electrochem. Soc.*, 2013, **160**, p D137–D145
21. A. Adloo, M. Sadeghi, M. Masoomi, and H.N. Pazhooh, High Performance Polymeric Bipolar Plate Based on Polypropylene/Graphite/Graphene/Nano-carbon Black Composites for PEM Fuel Cells, *Renew. Energy*, 2016, **99**, p 867–874
22. J. Chen, X. Cui, K. Sui, Y. Zhu, and W. Jiang, Balance the Electrical Properties and Mechanical Properties of Carbon Black Filled Immiscible Polymer Blends with a Double Percolation Structure, *Compos. Sci. Technol.*, 2017, **140**, p 99–105
23. S.S. Mirhosseini, R.S. Razavi, M. Taheran, and M. Barekat, Wear Behavior of Polyurethane/Carbon Black Coatings on 6061 Aluminum Alloy Substrates, *Prog. Org. Coat.*, 2016, **97**, p 37–43
24. X. Liu, C. Wu, and X. Wang, Synthesis, Characterization, and Infrared-Emissivity Study of Ni-P-CB Nanocomposite Coatings by Electroless Process, *J. Coat. Technol. Res.*, 2010, **7**, p 659–664
25. A. Zarebidaki and S.-R. Allahkaram, Effect of Surfactant on the Fabrication and Characterization of Ni-P-CNT Composite Coatings, *J. Alloys Compd.*, 2011, **509**, p 1836–1840
26. Z.-Q. Meng, X.-B. Li, Y.-J. Xiong, and J. Zhan, Preparation and Tribological Performances of Ni-P-Multi-walled Carbon Nanotubes Composite Coatings, *Trans. Nonferrous Met. Soc. China*, 2012, **22**, p 2719–2725
27. Z. Gao, S. Zhao, Y. Wang, X. Wang, and L. Wen, Corrosion Behavior and Wear Resistance Characteristics of Electroless Ni-P-CNTs Plating on Carbon Steel, *Int. J. Electrochem. Sci.*, 2015, **10**, p 637–648
28. A. Simões, D. Battocchi, D. Tallman, and G. Bierwagen, Assessment of the Corrosion Protection of Aluminium Substrates by a Mg-Rich Primer: EIS, SVET and SECM Study, *Prog. Org. Coat.*, 2008, **63**, p 260–266
29. A. Singh, K.R. Ansari, A. Kumar, W. Liu, C. Songsong, and Y. Lin, Electrochemical, Surface and Quantum Chemical Studies of Novel Imidazole Derivatives as Corrosion Inhibitors for J55 Steel in Sweet Corrosive Environment, *J. Alloys Compd.*, 2017, **712**, p 121–133
30. Y. González-García, G.T. Burstein, S. González, and R.M. Souto, Imaging Metastable Pits on Austenitic Stainless Steel In Situ at the Open-Circuit Corrosion Potential, *Electrochem. Commun.*, 2004, **6**, p 637–642
31. H. Ma, Y. Gu, S. Liu, J. Che, and D. Yang, Local Corrosion Behavior and Model of Micro-arc Oxidation HA Coating on AZ31 Magnesium Alloy, *Surf. Coat. Technol.*, 2017, **331**, p 179–188
32. Y. Yin, L. Niu, M. Lu, W. Guo, and S. Chen, In Situ Characterization of Localized Corrosion of Stainless Steel by Scanning Electrochemical Microscope, *Appl. Surf. Sci.*, 2009, **255**, p 9193–9199
33. Y. Yuan, L. Li, C. Wang, and Y. Zhu, Study of the Effects of Hydrogen on the Pitting Processes of X70 Carbon Steel with SECM, *Electrochem. Commun.*, 2010, **12**, p 1804–1807
34. J.N. Balaraju, S.M. Jahan, and K.S. Rajam, Studies on Autocatalytic Deposition of Ternary Ni-W-P Alloys Using Nickel Sulphamate Bath, *Surf. Coat. Technol.*, 2006, **201**, p 507–512
35. N. Esmaeili, J. Neshati, and I. Yavari, Corrosion Inhibition of New Thiocarbohydrazies on the Carbon Steel in Hydrochloric Acid Solution, *J. Ind. Eng. Chem.*, 2015, **22**, p 159–163
36. F. Wang, S. Arai, and M. Endo, The Preparation of Multi-walled Carbon Nanotubes with a Ni-P Coating by an Electroless Deposition Process, *Carbon*, 2005, **43**, p 1716–1721
37. Z. Yang, H. Xu, Y.-L. Shi, M.K. Li, Y. Huang, and H.-L. Li, The Fabrication and Corrosion Behavior of Electroless Ni-P-Carbon Nanotube Composite Coatings, *Mater. Res. Bull.*, 2005, **40**, p 1001–1009
38. J.N. Balaraju, T.S.N. Sankara Narayanan, and S.K. Seshadri, Structure and Phase Transformation Behaviour of Electroless Ni-P Composite Coatings, *Mater. Res. Bull.*, 2006, **41**, p 847–860
39. T. Rabizadeh, S.R. Allahkaram, and A. Zarebidaki, An Investigation on Effects of Heat Treatment on Corrosion Properties of Ni-P Electroless Nano-coatings, *Mater. Des.*, 2010, **31**, p 3174–3179
40. M. Sribalaji, P. Arunkumar, K.S. Babu, and A.K. Keshri, Crystallization Mechanism and Corrosion Property of Electroless Nickel Phosphorus Coating during Intermediate Temperature Oxidation, *Appl. Surf. Sci.*, 2015, **355**, p 112–120
41. T.S.N. Sankara Narayanan, I. Baskaran, K. Krishnaveni, and S. Parthiban, Deposition of Electroless Ni-P Grade Coatings and Evaluation of Their Corrosion Resistance, *Surf. Coat. Technol.*, 2006, **200**, p 3438–3445
42. N. Latha, V. Raj, and M. Selvam, Effect of Plating Time on Growth of Nanocrystalline Ni-P from Sulphate/Glycine Bath by Electroless Deposition Method, *Bull. Mater. Sci.*, 2013, **36**, p 719–727
43. N. Sridhar, K.U. Bhat, Effect of Deposition Time on the Morphological Features and Corrosion Resistance of Electroless Ni-High P Coatings on Aluminium, *J. Mater.*, 2013, **2013**, Article ID 985763
44. A. Hadipour, S.M. Monirvaghefi, and M.E. Bahrololoom, Electroless Deposition of Graded Ni-P Coating, *Surf. Eng.*, 2015, **31**, p 399–405
45. S. Xu, X. Hu, Y. Yang, Z. Chen, and Y.C. Chan, Effect of Carbon Nanotubes and Their Dispersion on Electroless Ni-P under Bump Metallization for Lead-Free Solder Interconnection, *J. Mater. Sci. Mater. Electron.*, 2014, **25**, p 2682–2691
46. C.-K. Lee, Comparative Corrosion Resistance of Electroless Ni-P/nano-TiO_2 and Ni-P/Nano-CNT Composite Coatings on 5083 Aluminum Alloy, *Int. J. Electrochem. Sci.*, 2012, **7**, p 12941–12954
47. A. Sadeghzadeh-Attar, G. Ayubikia, and M. Ehteshamzadeh, Improvement in Tribological Behavior of Novel Sol-Enhanced Electroless Ni-P-SiO_2 Nanocomposite Coatings, *Surf. Coat. Technol.*, 2016, **307**, p 837–848
48. S. Afroukhteh, C. Dehghanian, and M. Emamy, Preparation of Electroless Ni-P Composite Coatings Containing Nano-scattered Alumina in Presence of Polymeric Surfactant, *Prog. Nat. Sci. Mater. Int.*, 2012, **22**, p 318–325
49. D. Ekmeckci and F. Bülbul, Preparation and Characterization of Electroless Ni-B/Nano-SiO_2, Al_2O_3, TiO_2 and CuO Composite Coatings, *Bull. Mater. Sci.*, 2015, **38**, p 761–768
50. S. Eraslan and M. Ürgen, Oxidation Behavior of Electroless Ni-P, Ni-B and Ni-W-B Coatings Deposited on Steel Substrates, *Surf. Coat. Technol.*, 2015, **265**, p 693–695

51. L. Bonin and V. Vitry, Mechanical and Wear Characterization of Electroless Nickel Mono and Bilayers and High Boron-Mid Phosphorus Electroless Nickel Duplex Coatings, *Surf. Coat. Technol.*, 2016, **307**, p 957–962
52. C. Wang, Z. Farhat, G. Jarjoura, M.K. Hassan, and A.M. Abdullah, Indentation and Erosion Behavior of Electroless Ni-P Coating on Pipeline Steel, *Wear*, 2017, **376–377**, p 1630–1639
53. Y.F. Shen, W.Y. Xue, Z.Y. Liu, and L. Zuo, Nanoscratching Deformation and Fracture Toughness of Electroless Ni-P Coatings, *Surf. Coat. Technol.*, 2010, **205**, p 632–640
54. J. Alexis, C. Gaussens, B. Etcheverry, and J.-P. Bonino, Development of Nickel-Phosphorus Coatings Containing Micro Particles of Talc Phyllosilicates, *Mater. Chem. Phys.*, 2013, **137**, p 723–733
55. A. Ghasemi-Kahrizsangi, H. Shariatpanahi, J. Neshati, and E. Akbarinezhad, Corrosion Behavior of Modified Nano Carbon Black/Epoxy Coating in Accelerated Conditions, *Appl. Surf. Sci.*, 2015, **331**, p 115–126
56. Y. Suzuki, S. Arai, and M. Endo, Ni-P Alloy-Carbon Black Composite Films Fabricated by Electrodeposition, *Appl. Surf. Sci.*, 2010, **256**, p 6914–6917
57. G. Zhao and F. Deng, Electroless Plating of Ni-P-CNTs Composite Coating, *Key Eng. Mater.*, 2005, **280–283**, p 1445–1448
58. S.R. Allahkaram, M.H. Nazari, S. Mamaghani, and A. Zarebidaki, Characterization and Corrosion Behavior of Electroless Ni-P/Nano-SiC Coating Inside the CO_2 Containing Media in the Presence of Acetic Acid, *Mater. Des.*, 2011, **32**, p 750–755
59. H. Ashassi-Sorkhabi and M. Es'haghi, Corrosion Resistance Enhancement of Electroless Ni-P Coating by Incorportation of Ultrasonically Dispersed Diamond Nanoparticles, *Corros. Sci.*, 2013, **77**, p 185–193
60. M. Terada, A.F. Padilha, A.M.P. Simões, H.G. de Melo, and I. Costa, Use of SECM to Study the Electrochemical Behavior of DIN 1.4575 Superferritic Stainless Steel Aged at 475°C, *Mater. Corros.*, 2009, **60**, p 889–894
61. M. Zhao, Z.H. Qian, R.J. Qin, J.Y. Yu, Y.J. Wang, and L. Niu, In Situ SECM Study on Concentration Profiles of Electroactive Species from Corrosion of Stainless Steel, *Corros. Eng. Sci. Technol.*, 2013, **48**, p 270–275
62. J. Izquierdo, L. Martín-Ruíz, B.M. Fernández-Pérez, R. Rodríguez-Raposo, J.J. Santana, and R.M. Souto, Scanning Microelectrochemical Characterization of the Effect of Polarization on the Localized Corrosion of 304 Stainless Steel in Chloride Solution, *J. Electroanal. Chem.*, 2014, **728**, p 148–157